DOI: 10.61782/fa.2025.0438

FORUM ACUSTICUM
EURONOISE 2025

IDENTIFICATION OF AN ACTUATION MANIFOLD FOR OPEN-LOOP CONTROL OF SUBSONIC JET NOISE WITH ACOUSTIC-BASED EXCITATION

Luca Franceschelli* **Marco Raiola** **Andrea Ianiro** **Stefano Discetti**

Department of Aerospace Engineering, Universidad Carlos III de Madrid,
Avda. Universidad 30, Leganés, 28911, Madrid, Spain

ABSTRACT

Subsonic jet noise remains a key contributor to aircraft noise, particularly during takeoff. While reducing jet velocity has helped, further mitigation requires controlling turbulent structures in the shear layer, which are primary sound sources. Active jet control offers a promising solution with minimal efficiency loss. This study investigates acoustic-based actuation in a turbulent subsonic jet. Experiments are conducted in the jet facility of the anechoic chamber at Universidad Carlos III de Madrid. Acoustic excitation is provided by counter-facing loudspeakers in the stagnation chamber, following an open-loop control strategy. The goal of this work is to explore the actuation manifold produced by the acoustic excitation using data-driven dimensionality-reduction techniques. Isometric Mapping (ISOMAP) and Proper Orthogonal Decomposition (POD) are applied to phase-averaged velocity fields measured via Particle Image Velocimetry, phase-locked with the actuation. The impact of actuation is further assessed using hydrodynamic pressure measurements in the shear layer and acoustic pressure in the far field. Results confirm the existence of an actuation manifold in the phase-averaged velocity fields. The influence of actuation on the jet is further supported by both shear-layer and far-field pressure measurements.

Keywords: Jet noise, Reduced Order Modelling, ISOMAP, flow control

**Corresponding author*: lfrances@ing.uc3m.es.

1. INTRODUCTION

Jet noise is a major contributor to aircraft noise pollution, particularly during takeoff and landing. Although advances in engine design and reductions in jet exhaust velocity have led to significant improvements, further noise reduction requires direct control of the turbulent structures in the jet shear layer, which are the primary sources of subsonic jet noise. Among emerging strategies, active flow control using acoustic excitation has shown promise in modifying the jet dynamics with minimal aerodynamic penalties [1].

Reduced-Order Modeling (ROM) has become central in the analysis and control of such complex flows. Classical techniques like Proper Orthogonal Decomposition (POD) offer a linear, energy-optimal decomposition of flow fields, providing compact representations useful for modeling and control [2, 3]. However, the inherently nonlinear behavior of turbulent and transitional jets often limits the effectiveness of such linear approaches in capturing the full extent of flow dynamics.

To overcome these limitations, nonlinear manifold learning methods aim to identify low-dimensional embeddings that reflect the true geometry of high-dimensional flow data. Isometric mapping (ISOMAP) [4], which preserves geodesic distances between flow snapshots, has recently shown promise in uncovering coherent structures in complex shear flows [5]. Compared to POD, ISOMAP has demonstrated better separation of flow regimes in experimental settings [6]. Furthemore, Marra et al. [7] have demonstrated that ISOMAP can be used to unveil "actuation manifolds", i.e., manifolds of flows under different types of actuations, with interpretable coordinates.

In this work, we apply ISOMAP to experimental data

from an acoustically-excited subsonic jet in a transitional regime, at $Re = 10,000$ (with the Reynolds number Re being based on the bulk jet velocity U_j and the nozzle diameter D). Open-loop actuation is applied via counter-facing loudspeakers mounted in the stagnation chamber, operating in phase. Measurements of the velocity field are acquired using Particle Image Velocimetry (PIV). Additionally, synchronized acoustic measurements using two sets of microphones are performed: four placed along the jet axis in the near field to track the evolution of pressure fluctuations, and two in the far field positioned at 30° and 90° relative to the jet axis. Synchronization with the actuation signal enables the computation of phase-averaged flow fields, capturing several phases of each periodic control actuation. The ability of ISOMAP to identify a low-dimensional actuation manifold in both turbulent and transitional regimes is assessed on phase-averaged flow fields. Results are compared with those obtained using POD, highlighting the advantages of nonlinear manifold learning in revealing coherent flow structures under periodic forcing. A similar analysis performed on the near- and far-field microphone temporal signals, however, failed in identifying a low-dimensional manifold, not providing a conclusive answer to whether a control manifold exists for the instantaneous noise measurements.

2. METHODOLOGY

The actuation manifold is identified using the ISOMAP algorithm, a nonlinear dimensionality-reduction technique that seeks to uncover a low-dimensional embedding that preserves geodesic distances between flow snapshots in a high-dimensional feature space. This section outlines the core steps of the methodology, which are further detailed in [7].

Let us consider a collection of M snapshots, each represented as a high-dimensional vector $\mathbf{u}_i \in \mathbb{R}^d$. The first pairwise distances between snapshots using the standard Euclidean norm are equal to:

$$\|\mathbf{u}_i - \mathbf{u}_j\| = \left(\sum_{m=1}^{d} \left| u_i^{(m)} - u_j^{(m)} \right|^2 \right)^{1/2}. \quad (1)$$

A neighborhood graph is constructed by connecting each snapshot to its k-nearest neighbors according to the Euclidean distance. The geodesic distances between all pairs of snapshots are then estimated as the shortest paths on this graph. The resulting geodesic distance matrix $\boldsymbol{D}_{\mathrm{G}} \in \mathbb{R}^{M \times M}$ approximates the manifold distances and serves as the basis for the embedding.

Classical multidimensional scaling (MDS) is then applied to compute the low-dimensional embedding $\Gamma = (\tilde{\gamma}_{ij})_{1 \le i \le M,\, 1 \le j \le n} \in \mathbb{R}^{M \times n}$. The optimal set of coordinates is obtained from the eigenvectors corresponding to the largest n eigenvalues of the double-centered squared distance matrix. Each snapshot $\mathbf{u}_i$ is mapped to $\boldsymbol{\gamma}_i \in \mathbb{R}^n$, preserving its geodesic relationships with other samples.

The quality of the embedding is evaluated using the *residual variance*, R_v, which measures how faithfully the embedding represents the geometry of the original dataset.

In this work, the ISOMAP algorithm is applied to a velocity field ensemble including 20 phase-averaged fields for each actuation at a distinct frequency, yielding a closed trajectory in the reduced-order manifold that captures the system's coherent response to forcing. ISOMAP has also been tested on portions of the time signal provided by the 2 sets of microphones. In this latter case no coherent trajectory has been identified in the reduced-order manifold, leaving open the question if a control manifold can be identified for the non-phase-averaged data.

3. EXPERIMENTAL SET-UP

The experiments are conducted in the jet facility located inside the anechoic chamber of Universidad Carlos III de Madrid [8]. The setup consists of an air jet issuing from a round nozzle with exit diameter $D = 10\,\mathrm{mm}$. The jet flow condition investigated correspond to a transitional jet at Reynolds number $Re = 10{,}000$, with natural transition inside the nozzle.

Open-loop acoustic forcing is applied in both cases using two counter-facing loudspeakers mounted in the stagnation chamber. A purely sinusoidal excitation is imposed through the loudspeakers at a set of discrete actuation frequencies f, selected to span a typical range of Strouhal numbers, defined as $St = fD/U_j$. The explored range covers $St \in [0.05, 1.2]$, with increments of 0.05. This corresponds to 24 actuation frequencies between 75 Hz and 1800 Hz. The acoustic signal is generated using two ND654 2 $\frac{1}{2}$" aluminum cone full-range drivers (4 Ω impedance), mounted in a counter-facing configuration. The input waveform is amplified using a Fosi Audio V1.0B stereo audio amplifier, and the output power supplied to the loudspeakers is fixed at 25 W. This configuration provides repeatable and robust acoustic excitation across the entire frequency range explored.

Two-component velocity fields are measured using

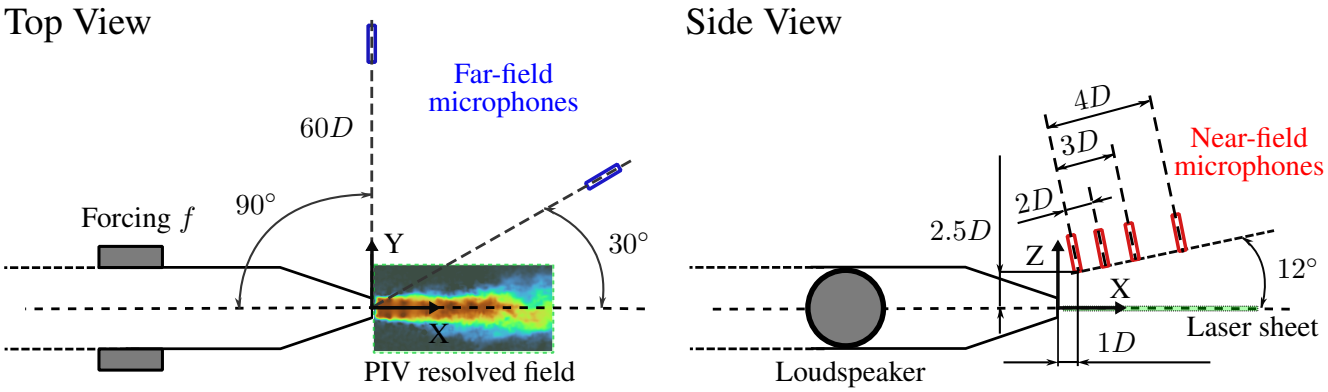

Figure 1: Sketch of the experimental setup. The top view (left) illustrates the positioning of the far-field microphones, while the side view (right) shows the placement of the near-field microphones.

PIV in the symmetry plane of the jet that intersects the axis of the two loudspeakers. The acquisition system consists of a 5.5 Mpx Andor Zyla sCMOS camera and a dual-cavity Nd:YAG laser operating up to 15 Hz with a pulse energy of 200 mJ. The flow is seeded with DEHS particles with a mean diameter of approximately 1 μm. The spatial resolution of the PIV setup is equal to 22.7 px/mm.

Image processing is performed using the PaIRS software developed at the University of Naples [9], with a final interrogation window of 32×32 px and 75% overlap. Optical reflections caused by the presence of four near-field microphones partially degrade the image quality. To mitigate this, a pre-processing step is applied to remove the background contribution. This is achieved using a POD-based technique, following the method described in [10], which enables efficient separation of the flow-induced particle signal from persistent light artifacts.

For each actuation frequency, phase-averaged velocity fields are obtained by synchronizing the non-temporally-resolved acquisition with the sinusoidal excitation signal. For each phase bin, 100 instantaneous velocity fields are recorded to ensure statistical convergence of the phase average. In total, 24 actuation frequencies are tested per flow condition, resulting in $M = 20 \times 24 = 480$ phase-averaged velocity fields for each case, which serve as the input for ISOMAP.

A rake of four Adafruit 1016 Electret Microphone Amplifier Boards (MAX4466) was installed in the near field, along with two GRAS 46AE microphones positioned in the far field. Microphone signals were acquired synchronously with both the actuation signal and the PIV system, at a sampling frequency of 200 kHz. A schematic of the experimental arrangement is shown in figure 1. The near-field microphones were arranged linearly along the jet development direction, inclined at 12° with respect to the jet axis. They were positioned at streamwise distances of 1, 3, 6, and 10 nozzle diameters D from the jet exit and mounted in a plane perpendicular to the PIV measurement plane. The far-field microphones were placed at a distance of $60D$ from the nozzle exit: one at an angle of 90° and the other at 30° relative to the jet axis.

4. RESULTS

To ensure consistent scaling across the dataset and enable meaningful comparison across different forcing conditions, the fluctuating phase-averaged velocity components u and v are normalized independently by their respective root-mean-square (rms) values, computed for each actuation case:

$$\bar{u} = \frac{u_{\text{PIV}}}{\text{rms}(u)}, \qquad \bar{v} = \frac{v_{\text{PIV}}}{\text{rms}(v)} \tag{2}$$

The ISOMAP and POD algorithms are then applied to the resulting normalized velocity field $\bar{\boldsymbol{u}} = [\bar{u}, \bar{v}]$, allowing for consistent low-dimensional analysis across the full range of forcing frequencies. This normalization prevents the dimensionality reduction methods from being biased toward actuation cases with inherently larger fluctuation amplitudes, ensuring that all cases contribute comparably to the extracted flow structures.

Before analyzing the embedding results in detail, we first assess the dimensionality reduction behavior of the two methods. Figure 2 compares the ISOMAP resid-

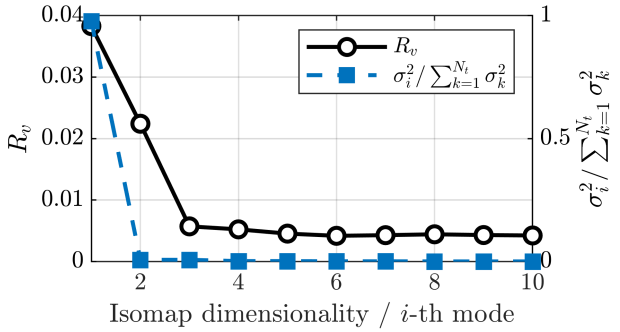

Figure 2: Comparison of dimensionality reduction: ISOMAP residual variance R_v (black) versus normalized POD eigenvalues $\sigma_i^2 / \sum \sigma_k^2$ (blue).

ual variance R_v and the normalized POD eigenvalues $\sigma_i^2 / \sum_k \sigma_k^2$ as functions of the mode index.

To further compare the effectiveness of the two methods, Figure 3 shows the pairwise projections of the first four low-dimensional coordinates obtained from ISOMAP (a) and POD (b), applied to the normalized fluctuating velocity fields. Each point corresponds to a phase-averaged snapshot and is color-coded by the Strouhal number St of the forcing. A neighborhood size of $k = 10$ is used for ISOMAP.

While POD succeeds in compressing the dataset energy into a few dominant modes, the resulting embedding fails to organize the snapshots coherently across the Strouhal number range. As shown in Figure 3b, the projections exhibit partial circular arrangements in the ψ_2-ψ_3 plane, which are reminiscent of phase-resolved dynamics for certain intermediate actuation frequencies. However, this structure fades significantly at low St, leading to a disordered and overlapping distribution of snapshots, where phase information is lost and actuation cases become indistinguishable.

In contrast, ISOMAP yields a more structured and physically interpretable embedding, as shown in Figure 3a. The pairwise projections of the first four coordinates reveal organized manifolds with clear geometric patterns—such as rings, spirals, and bifurcated surfaces—that consistently vary with the forcing frequency. Unlike POD, ISOMAP preserves the continuity of the phase trajectories even at low St, highlighting its ability to retain the intrinsic geometry of the flow dynamics and to represent both temporal evolution and actuation mechanisms in a unified low-dimensional space.

The contrast between actuation regimes is further explored by examining the flow structures associated with representative Strouhal numbers. Figure 4 shows the first spatial POD mode ϕ of the streamwise velocity fluctuations for three selected cases: $St = 0.15$, $St = 0.45$, and $St = 1$. The modes are normalized by $\sqrt{N_p}$, where N_p is the number of grid points. In the low-St case (top), the spatial mode reveals large-scale, nearly steady structures that extend over several jet diameters, reflecting a strong mean-flow pumping effect. At higher St, the modes become increasingly compact and periodic, with the $St = 1$ case (bottom) dominated by wave-like features consistent with Kelvin–Helmholtz vortices synchronized with the actuation.

To further investigate the flow response at different forcing frequencies, the phase-averaged voltage signals recorded from four near-field microphones are presented in Figure 5, for actuation cases $St = 0.15$, 0.45, and 1. The microphones are aligned along the jet centerline at axial distances of $1D$, $3D$, $6D$, and $10D$ from the nozzle exit (top to bottom).

At $St = 0.15$, the signals exhibit high-amplitude oscillations with a smooth and coherent phase shift across the microphones. The temporal behavior of the signals show a strong modulation, differing from the expected sinusoidal behavior typical of travelling waves. This pattern maintains its structure and shifts without significant deformation — likely driven by acoustic resonance within the facility. For $St = 0.45$ and $St = 1$, the voltage signals are significantly weaker but still exhibit low-amplitude oscillations. Interestingly, the waveform remains nearly unchanged across the four microphones, indicating limited spatial evolution and suggesting the presence of weak convective fluctuations rather than amplified coherent structures. In contrast, the $St = 0.15$ case shows strong spatial modulation of the waveform, with amplitude decreasing notably by $10D$, consistent with a resonance-driven wave confined to the near-nozzle region.

These findings reinforce the interpretation that the low-St regime excites a distinct, facility-driven mechanism with a strong near-field signature. This behavior differs fundamentally from the convective responses at higher frequencies, and explains why POD struggles to represent both within a common basis. ISOMAP, on the other hand, successfully embeds this physical variation into its low-dimensional manifold.

Finally, Figure 6 presents the power spectral density (PSD) of the far-field pressure signals acquired by the GRAS microphones placed at 30° (Mic1) and 90° (Mic2)

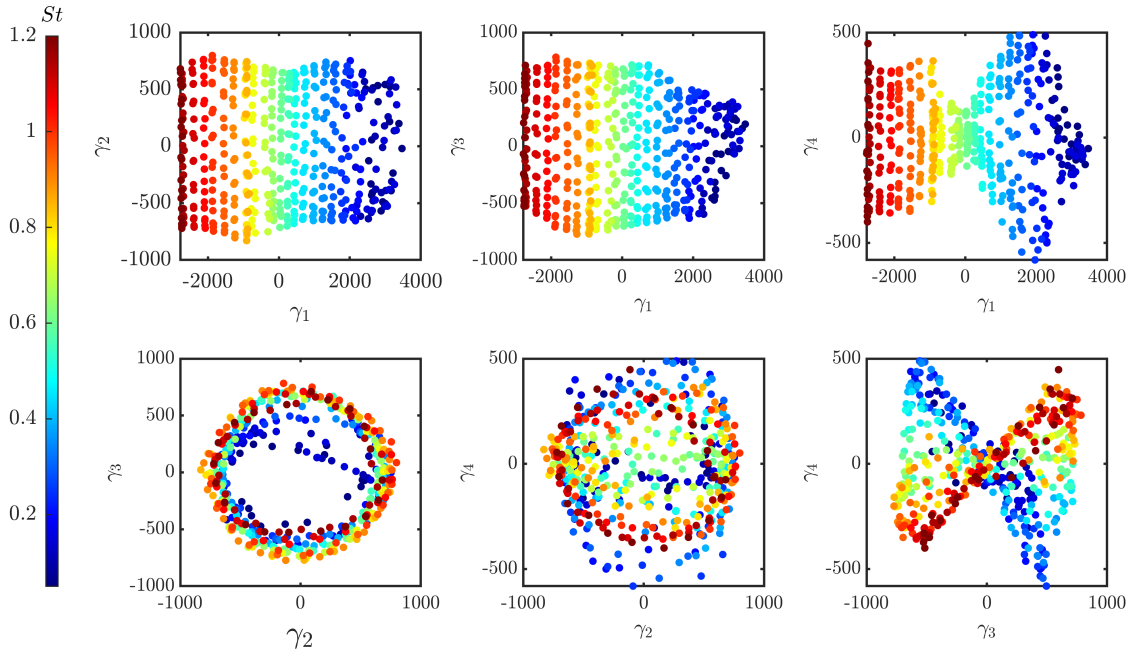

(a) ISOMAP

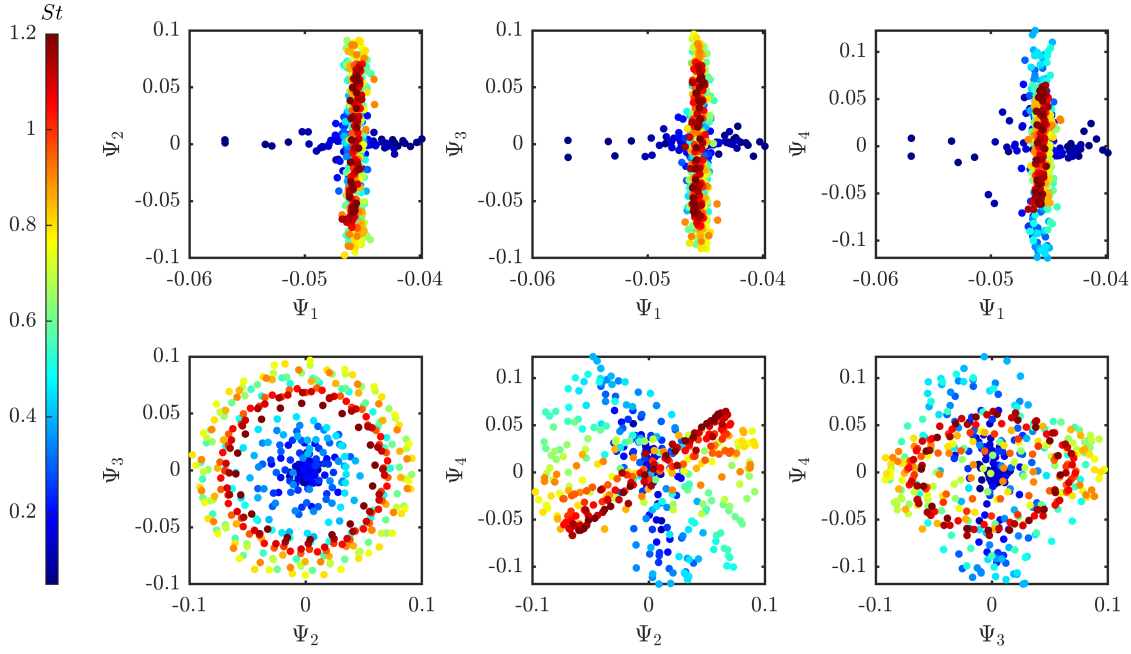

(b) POD

Figure 3: Pairwise projections of the first four low-dimensional coordinates obtained with ISOMAP **(a)** and POD **(b)**, applied to the normalized streamwise velocity fluctuations. Each point corresponds to a phase-averaged snapshot and is color-coded by the Strouhal number St. While POD compresses energy in a few modes, ISOMAP reveals a more structured and physically interpretable manifold.

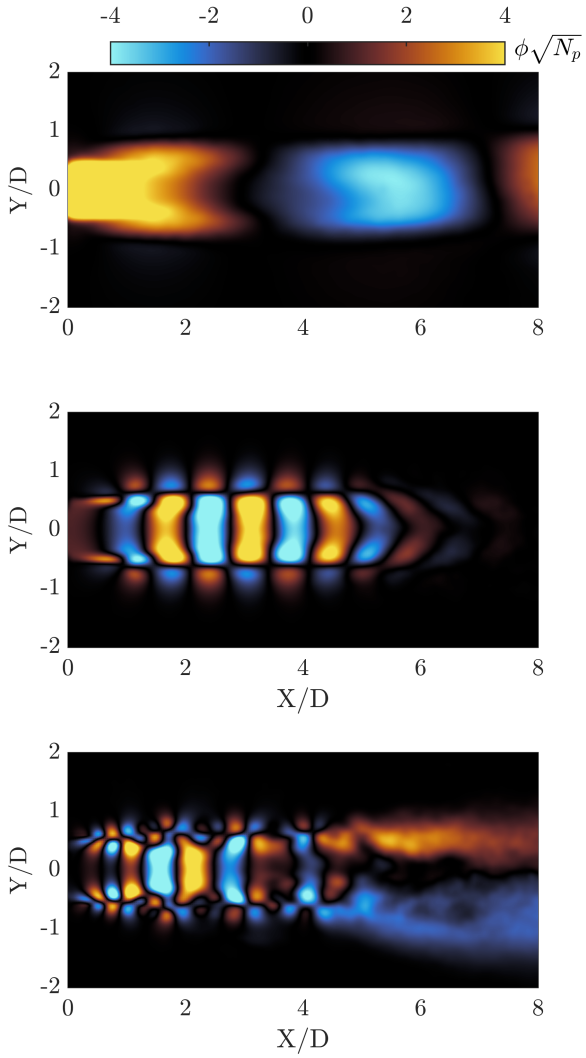

Figure 4: First spatial POD mode ϕ of the streamwise velocity fluctuations for the cases $St = 0.15$ (top), $St = 0.45$ (middle), and $St = 1$ (bottom). The modes are normalized by $\sqrt{N_p}$, where N_p is the number of grid points.

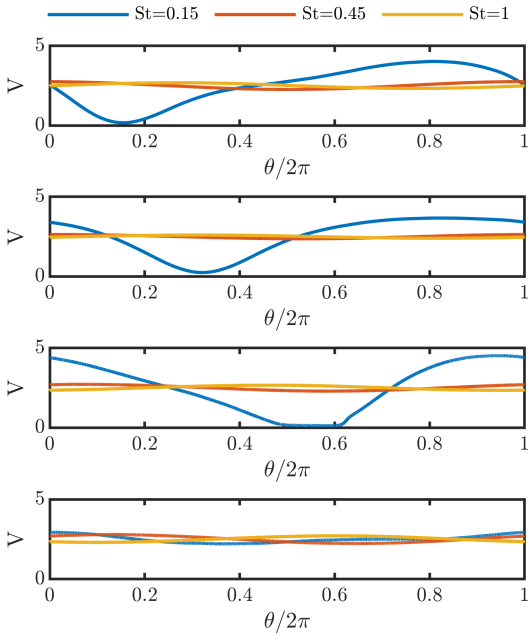

Figure 5: Phase-averaged voltage signals from four near-field microphones placed along the jet centerline at axial distances of $1D$, $3D$, $6D$, and $10D$ (top to bottom), for actuation cases $St = [0.15, 0.45, 1]$.

from the jet axis, comparing the uncontrolled and actuated cases at $St = 0.50$ and $St = 1.00$. The power spectra are plotted as Sound Pressure Levels (SPL), using a reference pressure of 20 μPa. The dominant peak observed in each actuated spectrum corresponds to the acoustic wave produced by the loudspeaker at the forcing frequency. However, the most informative effects of the actuation lie in the surrounding broadband spectral content. At 90° (Mic2), a substantial elevation of the high-frequency floor is observed in the actuated cases. This increase indicates enhanced radiation from small-scale turbulent structures, which typically dominate the side-radiated acoustic field [11]. In contrast, the spectra at 30° (Mic1) show more selective changes and are generally associated with sound generated by large-scale coherent structures aligned with the jet axis. These directional differences confirm that actuation not only injects tonal energy but also reorganizes the turbulence dynamics and their acoustic signatures in a frequency- and angle-dependent manner.

Overall, the results reveal that the acoustic impact of

actuation is far from trivial: while the forcing introduces energy at a specific tone, it also modifies the structure and distribution of broadband noise in ways that reflect deeper changes in the flow field. This complex interplay warrants further investigation to understand the link between actuation, turbulent structures, and jet noise generation mechanisms.

5. CONCLUSIONS AND FUTURE WORKS

The present work explores the existence of an actuation manifold for open-loop control of a subsonic transitional jet. The control action has been performed using acoustic excitation inside the stagnation chamber. Data-driven dimensionality reduction techniques have been applied to the phase-averaged velocity field measurements to identify the actuation manifold. Results shown the existence of a low-dimensional manifold for such data. The ISOMAP techniques, in particular, revealed to provide a more clear manifold than POD, being capable of coherently embedding different behaviors of the flow, i.e. "jet-pumping" mechanisms at low Strouhal numbers and Kelvin-Helmholtz vortices excitation at higher Strouhal numbers. The existence of a clear actuation manifold confirms the capability of the selected control action to affect the flow. This is further reinforced by the difference in behavior measured by both near-field microphones and the far-field microphones. Further work will focus in identifying a control manifold for non phase-averaged quantities.

6. ACKNOWLEDGMENTS

This work has been supported by the project EXCALIBUR, grant PID2022-138314NB-I00, funded by MCIN/AEI/10.13039/501100011033 and by "ERDF A way of making Europe".

7. REFERENCES

[1] A. Ginevsky, Y. V. Vlasov, E. V. Vlasov, and R. Karavosov, *Acoustic control of turbulent jets*. Springer Science & Business Media, 2004.

[2] G. Berkooz, P. Holmes, and J. L. Lumley, "The proper orthogonal decomposition in the analysis of turbulent flows," *Annual review of fluid mechanics*, vol. 25, no. 1, pp. 539–575, 1993.

[3] B. R. Noack, K. Afanasiev, M. Morzyński, G. Tadmor, and F. Thiele, "A hierarchy of low-dimensional models for the transient and post-transient cylinder wake," *Journal of Fluid Mechanics*, vol. 497, pp. 335–363, 2003.

[4] J. B. Tenenbaum, V. d. Silva, and J. C. Langford, "A global geometric framework for nonlinear dimensionality reduction," *science*, vol. 290, no. 5500, pp. 2319–2323, 2000.

[5] E. Farzamnik, A. Ianiro, S. Discetti, N. Deng, K. Oberleithner, B. R. Noack, and V. Guerrero, "From snapshots to manifolds–a tale of shear flows," *Journal of Fluid Mechanics*, vol. 955, p. A34, 2023.

[6] S. E. Otto and C. W. Rowley, "Inadequacy of linear methods for minimal sensor placement and feature selection in nonlinear systems: a new approach using secants," *Journal of Nonlinear Science*, vol. 32, no. 5, p. 69, 2022.

[7] L. Marra, G. Y. C. Maceda, A. Meilán-Vila, V. Guerrero, S. Rashwan, B. R. Noack, S. Discetti, and A. Ianiro, "Actuation manifold from snapshot data," *Journal of Fluid Mechanics*, vol. 996, p. A26, 2024.

[8] J. R. Moreno, L. Franceschelli, D. De la Prida, L. A. Azpicueta-Ruiz, and M. Raiola, "Implementation of a jet collector and dissipation cavity into a closed anechoic chamber for jet noise studies," in *30th AIAA/CEAS Aeroacoustics Conference (2024)*, p. 3066, 2024.

[9] G. Paolillo and T. Astarita, "Pairs-unina: A robust and accurate free tool for digital particle image velocimetry and optical camera calibration," in *Proceedings of 21st International Symposium on Applications of Laser and Imaging Techniques to Fluid Mechanics*, (Lisbon, Portugal), July 08–11 2024.

[10] M. A. Mendez, M. Raiola, A. Masullo, S. Discetti, A. Ianiro, R. Theunissen, and J.-M. Buchlin, "Pod-based background removal for particle image velocimetry," *Experimental Thermal and Fluid Science*, vol. 80, pp. 181–192, 2017.

[11] C. Tam, M. Golebiowski, and J. Seiner, "On the two components of turbulent mixing noise from supersonic jets," in *Aeroacoustics conference*, p. 1716, 1996.

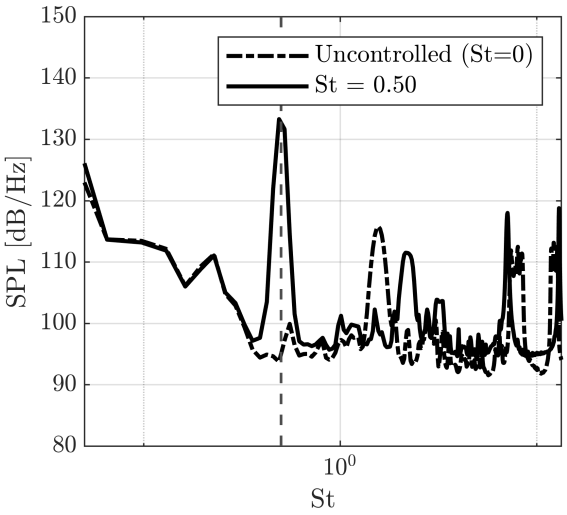

(a) Mic1 at 30°, $St = 0.50$.

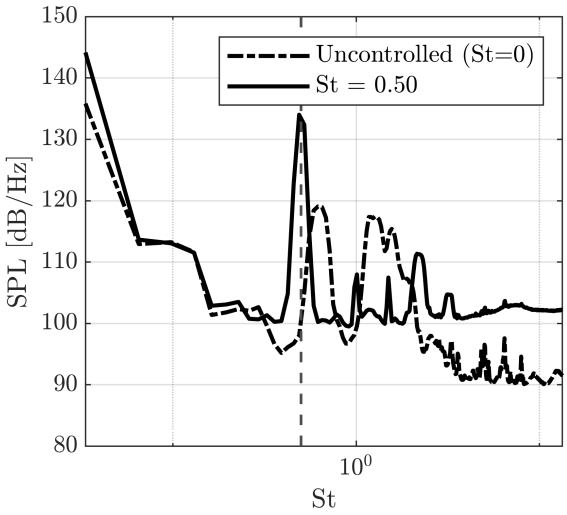

(b) Mic2 at 90°, $St = 0.50$.

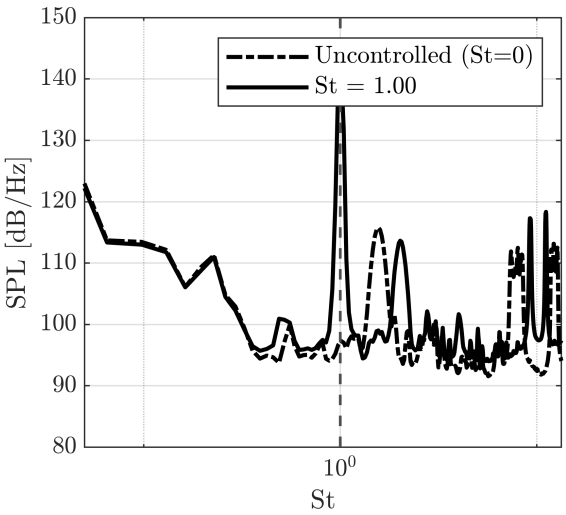

(c) Mic1 at 30°, $St = 1.00$.

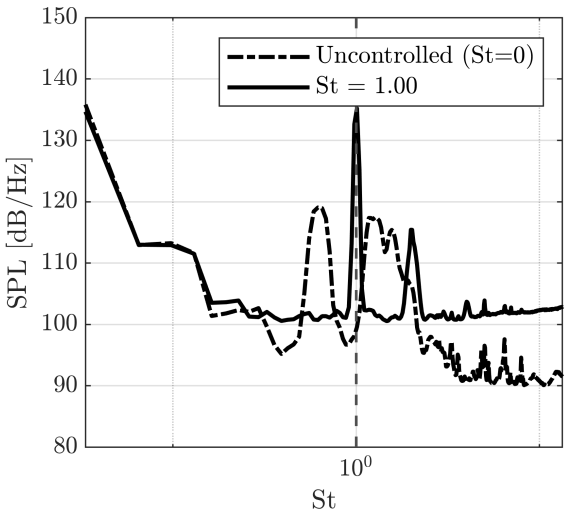

(d) Mic2 at 90°, $St = 1.00$.

Figure 6: Power spectral density (PSD) of far-field pressure signals measured by GRAS microphones at 30° (Mic1) and 90° (Mic2), comparing the uncontrolled case (dashed) with actuation at $St = 0.50$ and $St = 1.00$. Actuation introduces sharp tonal peaks and modifies the surrounding spectral distribution, highlighting complex, angle-dependent flow–acoustic interactions.